RESEARCH ARTICLE

WILEY

Partial-volume modeling reveals reduced gray matter in specific thalamic nuclei early in the time course of psychosis and chronic schizophrenia

Yasser Alemán-Gómez[1,2,3] | Elena Najdenovska[3,2,4] | Timo Roine[1,2,3] |
Mário João Fartaria[5,4,3] | Erick J. Canales-Rodríguez[4,2,6] | Zita Rovó[1] |
Patric Hagmann[2] | Philippe Conus[7] | Kim Q. Do[1] | Paul Klauser[1] |
Pascal Steullet[1] | Philipp S. Baumann[7,1] | Meritxell Bach Cuadra[3,2,4]

[1]Center for Psychiatric Neuroscience, Department of Psychiatry, Centre Hospitalier Universitaire Vaudois (CHUV) and University of Lausanne (UNIL), Lausanne, Switzerland

[2]Department of Radiology, Centre Hospitalier Universitaire Vaudois (CHUV) and University of Lausanne (UNIL), Lausanne, Switzerland

[3]Medical Image Analysis Laboratory (MIAL), Centre d'Imagerie BioMédicale (CIBM), Switzerland

[4]Signal Processing Laboratory (LTS5), Ecole Polytechnique Fédérale de Lausanne (EPFL), Lausanne, Switzerland

[5]Advanced Clinical Imaging Technology, Siemens Healthcare AG, Lausanne, Switzerland

[6]FIDMAG Germanes Hospitalàries Research Foundation, Sant Boi de Llobregat, Barcelona, Spain

[7]Service of General Psychiatry, Department of Psychiatry, Centre Hospitalier Universitaire Vaudois (CHUV) and University of Lausanne (UNIL), Lausanne, Switzerland

Correspondence
Yasser Alemán-Gómez and Meritxell Bach Cuadra, Department of Radiology, Centre Hospitalier Universitaire Vaudois (CHUV) and University of Lausanne (UNIL), Lausanne, Switzerland.
Email: yasseraleman@gmail.com (Y. A. G.) and meritxell.bachcuadra@unil.ch (M. B.C.)

Present address
Yasser Alemán-Gómez, Turku Brain and Mind Center, University of Turku, Turun yliopisto, Finland

Abstract

The structural complexity of the thalamus, due to its mixed composition of gray and white matter, make it challenging to disjoint and quantify each tissue contribution to the thalamic anatomy. This work promotes the use of partial-volume-based over probabilistic-based tissue segmentation approaches to better capture thalamic gray matter differences between patients at different stages of psychosis (early and chronic) and healthy controls. The study was performed on a cohort of 23 patients with schizophrenia, 41 with early psychosis and 69 age and sex-matched healthy subjects. Six tissue segmentation approaches were employed to obtain the gray matter concentration/probability images. The statistical tests were applied at three different anatomical scales: whole thalamus, thalamic subregions and voxel-wise. The results suggest that the partial volume model estimation of gray matter is more sensitive to detect atrophies within the thalamus of patients with psychosis. However all the methods detected gray matter deficit in the pulvinar, particularly in early stages of psychosis. This study demonstrates also that the gray matter decrease varies nonlinearly with age and between nuclei. While a gray matter loss was found in the pulvinar of patients in both stages of psychosis, reduced gray matter in the mediodorsal was only observed in early psychosis subjects. Finally, our analyses point to alterations in a sub-region comprising the lateral posterior and ventral posterior nuclei. The obtained results reinforce the hypothesis that thalamic gray matter assessment is more reliable when the tissues segmentation method takes into account the partial volume effect.

KEYWORDS

early psychosis, gray matter concentration, MRI, partial volume, pulvinar, schizophrenia, thalamus

1 | INTRODUCTION

The thalamus has a central role in the pathophysiology and psychopathology of schizophrenia as it forms a hub of several affected large-scale brain networks (Anticevic et al., 2014; Avram, Brandl, Bäuml, & Sorg, 2018; Woodward, Karbasforoushan, & Heckers, 2012) and is involved in functions compromised in the disorder such as perception, attention, arousal, emotion and cognitive processing (Byne, Hazlett, Buchsbaum, & Kemether, 2009). There is also cumulative evidence from connectomics that cerebral abnormalities in schizophrenia (SCHZ) tend to concentrate on the rich-club and its brain hub regions (Griffa et al., 2019; Klauser et al., 2016; van den Heuvel et al., 2013). Despite its relatively small size of ~8 cm^3 per hemisphere, the thalamus is a heterogeneous and complex structure. It is composed of several topographically organized nuclei, each of them having precise cortical and subcortical connections and mediating specific functions (Jones, 1985; Sherman & Guillery, 2006). The implication of the thalamus in SCHZ is supported by both neuropathology and structural and functional neuroimaging studies (Cho et al., 2018; Dorph-Petersen & Lewis, 2017; Marenco et al., 2012; Pergola, Selvaggi, Trizio, Bertolino, & Blasi, 2015; Steullet, in press; Woodward et al., 2012; Woodward & Heckers, 2016) which strongly suggest that anomalies are not evenly distributed across the thalamic nuclei, with some of the higher-order nuclei (i.e., mediodorsal, pulvinar) being the most affected. Postmortem studies of these nuclei have reported smaller volume and lower number of neurons and/or oligodendrocytes in SCHZ patients as compared with healthy individuals (Byne et al., 2009; Dorph-Petersen & Lewis, 2017). However, there is a large discrepancy in findings across postmortem studies (Dorph-Petersen & Lewis, 2017).

Structural Magnetic Resonance Imaging (MRI) studies in SCHZ based on T1-weighted (T1w) imaging have mainly analyzed the thalamus as a whole, with the aim of characterizing its volume and shape. Meta-analyses have revealed a significant mean volume reduction in both first-episode and chronic patients (Adriano, Spoletini, Caltagirone, & Spalletta, 2010; Brugger & Howes, 2017; Haijma et al., 2013) but also a great variability in thalamic volume (Brugger & Howes, 2017). This has been further corroborated by two large-scale multi-site consortium studies showing that the thalamus is in the top three of subcortical structures which have reduced size as compared with healthy control subjects (Okada et al., 2016; van Erp et al., 2016). Nevertheless, this volume decrease in patients with psychosis does not occur homogeneously along the thalamic anatomy. Based on shape analysis of the thalamic surface, different studies showed a surface deflation, which indicates a smaller volume in the anterior, mediodorsal and posterior parts in patients with psychosis when compared with healthy controls (Danivas, Kalmady, Venkatasubramanian, & Gangadhar, 2013; Janssen et al., 2012; Qiu, Zhong, Graham, Chia, & Sim, 2009; Smith et al., 2011).

Another meta-analysis of voxel-based morphometry (VBM) studies also show a significant decrease in gray matter (GM) density within the thalamus of patients (Glahn et al., 2008), an observation supported by a recent investigation on large cohorts of subjects suffering from SCHZ (Maggioni et al., 2017). In first-episode patients, however, a decreased thalamic GM volume is not clearly established (Chan, Di, McAlonan, & Gong, 2011; Huang et al., 2015). Furthermore, thalamic shape assessment and VBM analyses of GM (Pergola et al., 2015) point here again to structural alterations that are not evenly distributed across all nuclei.

Very few MR imaging studies have however investigated thalamic nuclei in SCHZ, mostly due to technical and methodological challenges regarding a reliable identification of specific thalamic subregions using conventional MRI techniques. Some studies have depicted different regions of interest within the thalamus mostly by manual segmentation of thalamic subregions (Buchmann et al., 2014; Cobia et al., 2017; Kemether et al., 2003) or by registering an anatomical atlas with patient MRI (Pergola et al., 2017). These approaches have revealed abnormalities in the mediodorsal and posterior parts of the thalamus. However, to understand the role and specificity of thalamus anomalies along the course of the disorder, from the prodromal stage to the chronic phase of SCHZ, it is essential to define more accurately the structural organization of individual thalamic nuclei, and to improve our methods of GM assessment.

MRI analyses of deep brain structures such as the thalamus is challenging due to the presence of multiple tissues within a single voxel. This phenomenon, known as partial volume (PV) effect complicates the tissue segmentation process which hampers accurate brain structure quantification. PV is particularly present in the thalamus because: (a) thalamic borders do not have a clear intensity contrast from the surrounding anatomical structures and (b) although considered as a deep GM region, the thalamus is also compounded by white matter (WM) tissue given the dense thalamocortical tracts innervating its nuclei (Morel, Magnin, & Jeanmonod, 1997). Thus, PV modulates the MR signal within the thalamus due to the presence of neuronal fibers in varying amounts. The PV effect (PVE) is well-known in the context of brain tissue segmentation techniques from MRI images (Tohka, 2014). It has been demonstrated that ignoring its presence might lead to significant errors in the tissue volume estimation measures (Cuadra, Cammoun, Butz, Cuisenaire, & Thiran, 2005; González Ballester, Zisserman, & Brady, 2002). However, to our knowledge, MRI studies of the thalamus in SCHZ have so far neglected the PV (Glahn et al., 2008; Pergola et al., 2015).

In the current study, we aim to assess, by taking into account the PV, the GM tissue within the thalamus, and its subregions of subjects in the early phase of psychosis (EP) and in patients with chronic schizophrenia. Our first contribution is a comprehensive comparison

of the PV within the thalamus based on six different tissue segmentation techniques. Specifically, we performed the GM segmentation through approaches that explicitly estimate PV concentrations (FAST (Zhang, Brady, & Smith, 2001), NISEG (Roche, 2016) and ATROPOS (Avants, Tustison, Wu, Cook, & Gee, 2011)), and also with methods that treat PV effect indirectly (ATROPOS without modeling PV "ATROPOS-NOPV", SPM8 and SPM12 [Ashburner & Friston, 2005]). We hypothesized that techniques that explicitly model the partial volume would capture more accurately thalamic differences in GM between EP or SCHZ patients and healthy controls than techniques that implicitly account for PVE adding extra tissue classes. The second major contribution of our work is the analysis of GM at the thalamic level, based on an automated atlas-based segmentation approach which includes a probabilistic atlas of seven thalamic subregions per hemisphere (Najdenovska et al., 2018). Overall, our comparative study of thalamic GM was performed at three different anatomical scales: (a) within the whole thalamus, (b) at the thalamic subregions level, and (c) at a voxel-wise level.

2 | MATERIALS AND METHODS

2.1 | Participants

Twenty-three patients with chronic schizophrenia (*SCHZ*) and 41 patients within 5 years of a first psychotic episode, a period called "early psychosis" (*EP*) were recruited from the Service of General Psychiatry (Lausanne University Hospital, Switzerland) (see Table 1). Subjects with SCHZ met the DSM-IV criteria for schizophrenia or schizoaffective disorder (Association, 2000). Among the 23 chronic patients with a schizophrenia spectrum disorder, 21 were diagnosed with schizophrenia, 1 with schizoaffective disorder and 1 with delusion disorder. Patients in the early phase of psychosis were recruited from the TIPP Program (Treatment and Early Intervention in Psychosis Program, University Hospital, Lausanne, Switzerland) (Baumann et al., 2013) which is a 3 year program specialized in the treatment of early phase of psychosis for patients aged between 18 and 35 years old. The definition of "early" for duration of illness below 5 years was used to include all the participants involved in our 3-year clinical program. These criteria take into account that some of them agreed to participate in the imaging study at the end of the program and also had, potentially, a period of untreated psychosis before entering the clinical program.

All patients met threshold criteria for psychosis as defined by the "Psychosis threshold" subscale of the CAARMS (Yung et al., 2005). Symptomatic severity was assessed with the positive and negative syndrome scale (*PANSS*) (Kay, Fiszbein, & Opler, 1987) administered by a trained psychologist. All the patients were taking antipsychotic medication at the time of this study. The average medication, in chlorpromazine equivalent dose (*CPZ*) (Andreasen, Pressler, Nopoulos, Miller, & Ho, 2010), is presented in Table 1 for both groups of patients. Severity of disability and level of functioning were determined using the Global Assessment of Functioning (*GAF*, American

TABLE 1 Sociodemographic and clinical characteristics of early psychosis, chronic schizophrenia and their respective matched healthy controls

	HC_EP	EP	Statistics		HC_schz	SCHZ	Statistics	
	N = 42	N = 41	t / χ^2	p	N = 27	N = 23	t/χ^2	p
Mean age (years)[mean (SD)]	25.5 (5.7)	25.4 (6.1)	t = 0.04	.96	37.7 (7.8)	40.2 (9.0)	t = 2.61	.17
Gender (male/female)	28/14	26/15	χ^2 = 0	1	18/9	18/5	χ^2 = 0.83	.36
Handedness (right/left/others)	34/7/1	34/5/2	t = 0.036	.85	22/4/1	19/4/0	t = 0.34	.56
Duration of illness (days)[Mean (SD)][a]		754 (628)				5728 (2643)		
CPZ equivalent (mg) [Mean (SD)][b]		364 (321)				381 (290)		
PANSS positive[c]		13.9 (5.5)				15.13 (4.82)		
PANSS negative		15.1 (4.8)				16.41 (5.92)		
PANSS general		33.7 (9.9)				33.69 (9.95)		
GAF score[d]	82.9 (5.7)	60.9(6.9)	t = 12.2	<.01	83.1(4.4)	56.7(12.4)	t = 12.9	<.01

[a]Duration of illness was defined as the time between date of onset of first positive symptoms and date of scan acquisition.
[b]CPZ, antipsychotic medication intake in chlorpromazine equivalents at time of scanning (in mg).
[c]PANSS, positive and negative syndrome scale.
[d]GAF, global assessment of functioning scale.

Psychiatric Association) scale (Association, 2000). Sixty-nine healthy controls (*HC*), recruited from similar geographic and sociodemographic areas, were assessed by the Diagnostic Interview for Genetic Studies. Major mood, psychotic or substance-use disorder and having a first-degree relative with a psychotic disorder were exclusion criteria for healthy controls. HC were classified in two groups (HC$_{schz}$ and HC$_{ep}$ with 27 and 42 subjects, respectively) in order to match with the patients groups (schizophrenia and early psychosis) for gender, age and handedness. Neurological disorders and severe head trauma or mental retardation (IQ < 70) were exclusion criteria for all subjects. All the participants provided informed written consent for this study, and the procedure was approved by the Ethics Committee of Clinical Research of the Faculty of Biology and Medicine, University of Lausanne, Switzerland.

2.2 | MRI acquisitions

MRI scans were performed on a 3-Tesla scanner (MAGNETOM TrioTim, Siemens Healthcare, Erlangen, Germany) equipped with a 32-channel head coil. Each scanning session included a magnetization prepared rapid acquisition gradient echo (*MPRAGE*) *T1w* sequence and a spin-echo echo-planar imaging (*SE-EPI*) diffusion spectrum imaging (*DSI*) sequence. The MPRAGE-T1w images were acquired with echo time (*TE*) = 2.98 ms, repetition time (*TR*) = 2,300 ms, inversion time (*TI*) = 900 ms flip angle (*FA*) = 8°, field of view (*FOV*) = $160 \times 240 \times 256$ mm^3 and voxel size = $1 \times 1 \times 1.2$ mm^3. The DSI (q4half acquisition scheme) sequence included 1 b0 acquisition plus 128 diffusion weighted directions with echo time (*TE*) = 103 ms, repetition time (*TR*) = 5,900 ms, field of view (*FOV*) = $211 \times 211 \times 114$ mm^3, voxel size = $2.2 \times 2.2 \times 3$ mm^3 and maximum b-value = 8000s/mm^2. Acquisition times for both MPRAGE-T1w and DSI sequences were $\sim$7 and 13 min respectively. Subjects with MRI images containing artifacts were excluded from the study.

2.3 | Brain tissue segmentation

In the last years, various brain MRI segmentation techniques have been developed, comprising both supervised and nonsupervised approaches (Cuadra et al., 2005; de Boer et al., 2010; Despotović, Goossens, & Philips, 2015; Tohka, 2014). Among nonsupervised techniques, the Bayesian based approaches have been largely adopted for neuroimaging studies based on T1w MRI because they have demonstrated very good accuracy and reproducibility (Ashburner & Friston, 2005; Puonti, Iglesias, & Van Leemput, 2016; Van Leemput, Maes, Vandermeulen, & Suetens, 1999; Zhang et al., 2001). In the Bayesian framework the tissue posterior probability maps are often obtained via Maximum a posteriori (*MAP*) through the observed image intensities. These methods may include some prior information either from tissue probabilistic atlases (Ashburner & Friston, 2005) or local spatial priors (Van Leemput et al., 1999; Zhang et al., 2001) or both (Tohka, Dinov, Shattuck, & Toga, 2010). These *probability-based*

methods implicitly model the partial volume by incorporating extra tissue classes. By contrast, other algorithms (Manjón, Tohka, & Robles, 2010; Roche & Forbes, 2014; Shattuck, Sandor-Leahy, Schaper, Rottenberg, & Leahy, 2001; Tohka, 2014; Tohka, Zijdenbos, & Evans, 2004; Zhang et al., 2001) tackle the PV effect explicitly by using the *mixel* model (Choi, Haynor, & Kim, 1991). This model assumes that the intensity value in each image voxel is a weighted sum of random variables, each of which characterizes a pure tissue type (e.g., GM and WM.) Thus, they aim to estimate the tissue concentration proportions within each image voxel that generate the observed intensity rather that the probability that one tissue type is present in that voxel.

In this paper, the estimation of GM within the thalamus was performed by six different tissue segmentation methods: three concentration-based (NISEG (Roche, 2016), FAST (Zhang et al., 2001) and ATROPOS (Avants et al., 2011)) and three probability-based (ATROPOS without PV, SPM8 and SPM12 (Ashburner & Friston, 2005)). Preprocessed T1w MR images were taken as input for the different methods. In the preprocessing step, the images were corrected for field intensity inhomogeneities using N4 (Tustison et al., 2010) and the intracranial volume (*ICV*) was obtained using a skull striping algorithm (Koutsouleris et al., 2012).
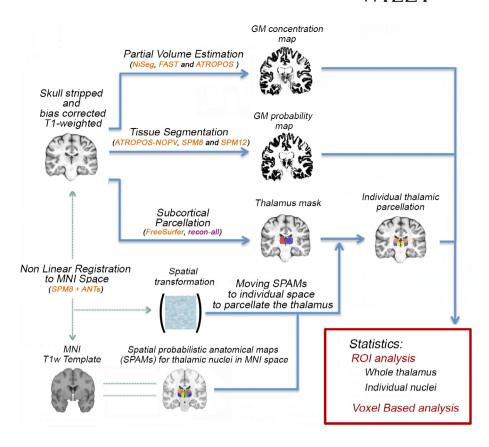
The overview of the imaging processing workflow is summarized in Figure 1 and the employed parameters, for each of the methods described here below, are detailed in section S6 of the Supplementary material.

2.4 | Concentration-based algorithms

2.4.1 | NISEG

This partial volume estimation method (Roche & Forbes, 2014) models the voxel intensity through the *mixel* model (Choi et al., 1991) by adding the cerebrospinal (*CSF*), GM and WM global characteristic intensities weighted by their respective local concentrations with a Gaussian noise with constant *SD* across tissues. Both tissue concentrations and global tissue parameters (mean and *SD* of the tissue intensity) are estimated through a maximum likelihood estimation approach that leads to an ill-posed problem and needs to be regularized. The authors (Roche & Forbes, 2014) propose to regularize the problem based on the three following assumptions: (a) voxels with mild PV are more frequent than those with strong PV, (b) estimated tissue concentration maps are spatially smooth, and (c) the existence of a large gap between global mean tissue intensities. NISEG has proved its accuracy in classification of Alzheimer disease and mild cognitive impairment patients compared with conventional brain morphometry methods (Roche & Forbes, 2014). This method also revealed diffuse pathology in deep brain nuclei structures, including the thalamus, in patients with multiple sclerosis (Bonnier et al., 2016). We used the publicly available NISEG software (Roche, 2016) with default parameters and initialization settings. An example of its resulting GM matter concentration map is shown in Figure 2b.

FIGURE 1 Image processing workflow summary. The estimation of gray matter within the thalamus is performed by using six different segmentation methods. The analysis is done at three different anatomical scales: whole thalamus, thalamic regions and voxel-wise

2.4.2 | FMRIB's Automated Segmentation Tool

The second segmentation algorithm based on PV is FMRIB's Automated Segmentation Tool (FAST) (Zhang et al., 2001). It is based on a probabilistic Hidden Markov Random Field (HMRF) model that combines observed tissue intensities with local spatial prior information encoded through the mutual influences of neighboring voxels. The algorithm iterates between the tissue class parameters (mean and SD), the tissue class label estimation (segmentation) and a bias field estimation via a three-step Expectation–Maximization (EM) (Van Leemput et al., 1999; Zhang, 1993) process. Finally, FAST derives PV tissue maps from a MRF-mixel type model. We used FAST with initial mean and variance estimation of three tissue classes (CSF, GM, and WM) based on histogram analysis (using the multiple Otsu's thresholding method, section IIIB in [Otsu, 1979]). This takes into account that each class should be widely separated from each other while at the same time having relatively low intraclass variances. Segmentation was performed using the default parameters and without probability tissue priors.

2.4.3 | ATROPOS

This open-source software proposes a general segmentation framework also based on the Bayesian formulation for a multivariate

segmentation problem. Similarly to FAST, ATROPOS incorporates a local spatial prior through Markov Random Fields to the classical finite mixture model (FMM) of the observed intensities. However, instead of using the Potts model (Zhang et al., 2001) for neighbors interaction, it uses a modified energy term (Noe & Gee, 2001) allowing neighborhood locations to be weighted more heavily than distant voxels. This allows smoother transitions between tissue types in favor of PV estimation. Similar to FAST, an iterative EM algorithm is used for tissue parameters (mean and variance) and tissue class label estimation. The use of the ATROPOS PV estimation option allows to model mixtures of classes within single voxels. We performed a three-tissue segmentation (CSF, GM, and WM) using k-means as initialization for tissue parameters and we modeled the PV effects between CSF/GM and GM/WM. Though ATROPOS can also incorporate tissue probabilistic maps into the mixing proportions, this option was not used.

2.5 | Probability-based algorithms

2.5.1 | ATROPOS-NOPV

We also run the ATROPOS segmentation method described above but without PV modeling in order to better evaluate the contribution of PV, that is, without any other methodological differences as compared with ATROPOS.
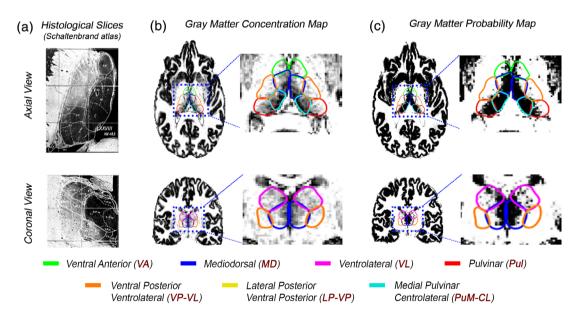
2.5.2 | SPM

The tissue segmentation method (New Segment) implemented in statistical parametric mapping (SPM) proposes a unified segmentation model that performs tissue segmentation, registration and intensity non-uniformity (bias) correction in the same model. As the methods previously described, this approach is based on a Bayesian MAP framework. Though it does not explicitly model the partial volume, it implicitly takes it into account by modeling each brain tissue class by a mixture of multiple Gaussian distributions, thus allowing non-Gaussian distribution per tissue class. In contrast to previous approaches, SPM segmentation does not estimate the mixing tissue concentration within a single voxel. Furthermore, it employs spatial tissue probability maps (Evans, Kamber, Collins, & MacDonald, 1994) as prior information to estimate the mixing proportions between tissue classes. These maps represent the spatial prior probability, in Montreal neurological institute (MNI) space, of each voxel to belong to any of these brain tissues. In the latest version of SPM (*SPM12*), the prior probability maps were obtained by averaging GM, WM, and CSF tissue segmentation images from healthy control subjects obtained from the IXI-database (http://brain-development.org/). The introduction of these new spatial probability maps led to notable differences in the GM priors probability of the deep brain nuclei as compared with the previous version included in SPM8 where different prior probability maps built from young healthy subjects from the MNI database were used. There exist also few other methodological differences between SPM8 and SPM12 such as the regularization in the registration step, the default settings and the new re-scaling step of the tissue probability maps.

In this work, in addition to SPM12, we also explored the previous version, SPM8, because it has been extensively used in neuroimaging studies of early psychosis and schizophrenia (Glahn et al., 2008). Both versions were applied using their default parameters. The estimated GM probability map using the SPM12 version of "New segment" is illustrated in Figure 2c.

2.6 | Tissue concentration versus probability

All the described segmentation methods provide output tissue-related maps with values that range between 0 and 1 (see Figure 2). However, the estimated PV tissue *concentration* (NISEG, FAST, ATROPOS) and the posterior *probability* tissue maps (ATROPOS-NOPV and both SPM methods) do not represent the same quantity. For instance, voxels with a high posterior probability to belong to a tissue type might have only an average concentration of that tissue. These differences can be observed when comparing GM concentration (illustrated with the NISEG method Figure 2b) and probability maps (displayed with the SPM12, Figure 2c). On one hand, as compared with GM probability, the GM concentration varies more smoothly within the whole thalamus. On the other hand, the GM probability shows sharper transitions between GM and WM, with values close to 1 (considered as GM) found in the most medial part of the thalamus and values close to 0 (considered as WM) elsewhere. This is in line with Manjón et al. (2010) who found that posterior probability segmentation methods lead to "rougher" tissue maps as compared with the ones resulting from methods that explicitly take into account the PV.

FIGURE 2 Qualitative results of GM estimation. (a) Images of histological axial (top) and coronal (bottom) sections stained for myelin from the Shalterbrand atlas (Schaltenbrand, Hassler, & Wahren, 1977). To help for comparisons with MRI images of GM, black and white have been inverted so the myelin staining is displayed in white. (b) Concentration of GM estimated by the NISEG algorithm. (c) GM probability obtained by the SPM12 tissue segmentation method. GM values in (b) and (c), which were obtained for the same subject, range from 0 (white) to 1 (black) and are displayed with equal window level. Regions of interest within the thalamus have been defined through atlas-based segmentation using a probabilistic atlas of the thalamic nuclei (Najdenovska et al., 2018)

2.7 | Gray matter quantification

In the following sections, we will denote GM concentration maps (from NISEG, FAST, and ATROPOS) and GM posterior probability maps (from ATROPOS-NOPV, SPM8, and SPM12) as *GMc* and *GMp*, respectively. Within each region of interest (left and right thalamus and their corresponding thalamic subregions) as defined below, we quantified the the GM volume and the mean GM. For each segmentation method, the GM volume was estimated by multiplying the voxel volume either with *GMc* or *GMp* maps and summing the values for all the voxels within the region of interest.

3 | REGIONS OF INTEREST

3.1 | Thalamus segmentation

For each subject, the left and right thalamus were segmented by combining T1w and diffusion-weighted MRI (*DWI*), following the method described in (Battistella et al., 2017). Sub-cortical regions were segmented from T1w images by using FreeSurfer (Fischl et al., 2002). A refinement step over the FreeSurfer thalamus segmentation was applied in order to remove CSF and WM voxels belonging to both the ventricles and the internal capsule. Such refinement step is supported by previous works (Battistella et al., 2017; Glaister et al., 2017) that demonstrated an improved thalamic border delineation when using multi-modal features (e.g., T1w/T2w, diffusion MRI, prior tissue probabilities). Specifically, in our study the voxels with CSF probability higher than 5% or those within a 2-mm distance from the border of the thalamic mask having fractional anisotropy (*FA*) values higher than 0.55 were removed from the original FreeSurfer binary mask of the thalamus. The CSF posterior probability maps were computed by using SPM12 (Ashburner & Friston, 2005) and the FA maps were obtained by applying a custom processing pipeline to DSI data. This custom workflow employed Mrtrix3 (Tournier, Calamante, & Connelly, 2012) and FSL (*FMRIB Software Library*) processing suites for performing the following steps: denoising, bias field correction (Tustison et al., 2010), intensity normalization, head motion correction (with gradient table rotation), eddy current and distortion correction (using field maps) (Rohde, Barnett, Basser, Marenco, & Pierpaoli, 2004) and linear registration of DWI to T1 space using FLIRT (Jenkinson, Bannister, Brady, & Smith, 2002; Jenkinson & Smith, 2001)). The corrected DSI data were used to obtain FA maps by applying the *dwi2tensor* and *tensor2metric* routines implemented in MrTrix3 to the diffusion weighted images with b-values lower than 1500 s/mm^2. These maps (CSF and FA) were only used for the thalamic mask refinement.

3.2 | Thalamic nuclei parcellation

Today, there are few available methods to automatically parcellate the thalamic nuclei based on local structural imaging features (Iglesias

et al., 2018; Najdenovska et al., 2018; Su et al., 2019). To our knowledge, none of them has previously been used for the GM analysis in early psychosis or schizophrenia. Pergola et al (Pergola et al., 2017) first analyzed GM within thalamus by eroding the thalamic subregions resulting from an atlas-based segmentation using the digitized version of Morel (Morel et al., 1997). In our study we relied on an in-house spatial probabilistic anatomical maps (*SPAMs*) (Najdenovska et al., 2018) of 14 thalamic subregions (seven per hemisphere) that was constructed from 67 healthy subjects from the Human Connectome Project (Rosen, Toga, & Weeden, 2012). We selected this parcellation method among other techniques as this probabilistic atlas was constructed from a higher number of subjects (67 as compared with 6 and 20 used in [Iglesias et al., 2018; Su et al., 2019] respectively) and with an age range closer to the subjects in our study.

Firstly, each individual skull-stripped T1w image was non linearly registered (Avants et al., 2010) to MNI space by using as target template the nonlinear version of the ICBM152 atlas (Evans, Janke, Collins, & Baillet, 2012; Fonov et al., 2011). Secondly, the inverse of the resulting spatial transformation was applied to the probabilistic atlas to map it into the subject space. Thirdly, the maximum likelihood parcellation was determined by identifying, at each voxel, the label with the greatest value in the warped probability maps. Finally, the voxels belonging to the maximum likelihood parcellation that were not included in the refined thalamus mask were removed from the final parcellation. This T1w MRI based thalamic nuclei segmentation demonstrated the same ability to encode the local variability within the thalamus as other approaches based on the local patient-specific features (Najdenovska et al., 2018).

Figure 1 (bottom) illustrates the atlas-based segmentation process together with a coronal view of the probabilistic thalamic nuclei atlas and the resulting thalamic nuclei segmentation for a single subject. Each thalamus was subdivided in the following seven regions (Figure 2): ventral anterior (*VA*), mediodorsal (*MD*), pulvinar (*Pul*), ventrolateral (*VL*), ventral posterior/ventrolateral group (*VP-VL*), lateral posterior/ventral posterior group (*LP-VP*), and medial pulvinar/centrolateral (*PuM-CL*). Based on the current literature, the MD, Pul, and PuM-CL subregions include most of the nuclei relevant to SCHZ.

3.3 | VBM

In addition to the region of interest analysis, which is conditioned by the parcellation of the thalamus in seven nuclei, a VBM approach was also performed to evaluate voxel-wise differences between patients and controls groups. This technique gives an even-handed and comprehensive assessment of anatomical differences throughout the whole thalamic anatomy. First, *GMc* and *GMp* maps were transformed into the MNI standard coordinate system using a symmetric diffeomorphic normalization method (Avants et al., 2010) that was selected as the top ranked registration procedure in terms of accuracy and precision in an evaluation study (Klein et al., 2009). Individual T1w images were nonlinearly registered to MNI space using the nonlinear version of the ICBM152 atlas (Evans et al., 2012; Fonov

et al., 2011) as target template. The resulting spatial transformations (Native-to-MNI) were then applied to the thalamic masks, *GMc* and *GMp* maps to spatially aligned them in MNI space. Nearest neighbor for the thalamic masks and BSpline for *GMc* and *GMp* were used as interpolation methods. Secondly, a modulation step was applied using the Jacobian of the warp field to correct for tissue volume changes during the spatial normalization. Voxel intensities were scaled by the amount of expansion or contraction that has occurred during spatial normalization, so that the total amount of "tissue" remains the same as in the original image. Finally, the normalized *GMc* and *GMp* images were then smoothed using a 8-mm FWHM kernel and fed into the statistical analysis. A probabilistic image of the thalamus in MNI space was built by averaging the warped thalamic masks. This probabilistic image was binarized to create a thalamic mask for the VBM analysis.

3.4 | Statistical analysis

Statistical analyses were performed by using the Statistics and Machine Learning Toolbox included in Matlab (v.R2018b).

3.5 | Whole thalamus and thalamic subregions

Nonparametric Spearman rank partial correlations were used to test the association with clinical variables and chlorpromazine equivalents and to identify possible confounders that should be included in the statistical model. To test for group differences in demographics and clinical variables (HC$_{ep}$ vs. EP and HC$_{schz}$ vs. SCHZ), Student's *t* tests were used for continuous variables and chi-squared (χ^2) tests for discrete categorical variables. The GM volume, the mean *GMc* and mean *GMp* values for each region of interest (whole thalamus and thalamic subregions) were corrected for age, gender and intracranial volume using multiple regression analyses (Sullivan, Rosenbloom, Serventi, & Pfefferbaum, 2004). Unstandardized residuals were saved and used in the main analyses. The General Linear Model (*GLM*) is based on a number of assumptions, including that the observed values have a linear, additive structure, and that the residuals of the model fit have the same variance and are normally distributed. Not all variables met all these requirements. To test whether group differences in mean *GMc* or *GMp* existed, pair-wise comparisons between healthy controls and patients groups were conducted using either Mann–Whitney U or Student's *t* test depending on the normality of the data as evaluated by a Shapiro test. In all analyses, a *p* < .05 (two-tailed) was considered significant after controlling for multiple comparisons using the False Discovery Rate (*FDR*) with q = 0.05 (Benjamini & Hochberg, 1995). Standardized effect sizes of the differences were also reported throughout Cohen's d values where *d* < 0.5, *d* > 0.5 and *d* > 0.8 represent a low, medium and strong effects respectively. Mean and confidence intervals (α = 0.95) for the Cohen's d values were computed over 5,000 bootstrap samples. The bootstrap sampling technique was implemented using the MATLAB's (R2018b) functions "bootstrap" and "bootci" where only the 80% (with replacement) of the subjects from each group (HC$_{ep}$ (N = 33), HC$_{schz}$ (N = 21),

EP (N = 32) and SCHZ (N = 18)) was randomly selected in each of the 5,000 bootstrap iterations.

A quadratic model was fitted to investigate the possible nonlinear relationship between age and regional GM volumes for both psychotic patients and healthy controls (Cropley et al., 2016). For this analysis, early psychosis and schizophrenia patients were compared with their respective matched healthy controls.

3.6 | Voxel-based statistics

A GLM was used to explore voxel-wise differences where age, gender and ICV were included as non-explanatory co-regressors. A binary image including both thalami was used to restrict the analysis only to the voxels within the thalamus. Nonparametric statistics were performed using *randomize* (FMRIB Software Library) with 5,000 permutations and a threshold free cluster enhancement (*TFCE*) approach. Statistical parametric maps were generated and only voxels with *p* < .05 (fully corrected using the family-wise error) were considered as significant.

4 | RESULTS
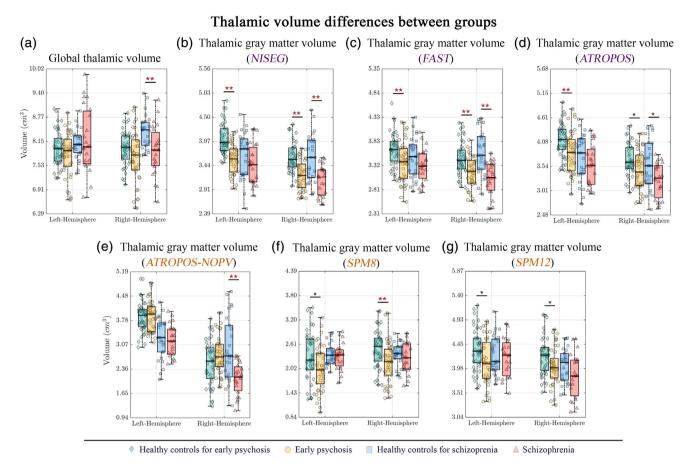
4.1 | Demographic and clinical differences

Groups were well matched for age, gender and handedness (Table 1) and no significant differences were found between groups in any of these variables (HC$_{ep}$ vs. EP: *p* = .96, *p* = 1 and *p* = .85. HC$_{schz}$ vs. SCHZ: *p* = .17, *p* = .36, and *p* = .56, respectively). As expected, healthy controls showed a significantly higher GAF scores than EP and SCHZ groups (*p* < .01).

4.2 | Whole thalamus

4.2.1 | Total and GM volume

The whole thalamus of EP and SCHZ patients was first compared with that of their respective matched controls by using two different measures: (a) the total volume of the thalamus from the refined thalamus mask, and (b) the GM volume by multiplying the voxel volume either with *GMc* or *GMp* maps and summing the values for all the voxels withinthe region of interest. (see Figure 3 and Table 2).

A reduced thalamic volume was found in the right thalamus of SCHZ patients only (*p* = .0029, *d* = 0.91, see Figure 3a). However, stronger differences between groups emerged when comparing the GM thalamic volume, in particular when the concentration-based algorithms were used. A significant thalamic GM volume reduction in the right hemisphere of both cohorts of patients as compared with their respective control subjects was found using NISEG (see Figure 3b, HC$_{ep}$ vs. EP: *p* < .0001, *d* = 1.24 and HC$_{schz}$ vs. SCHZ: *p* = .0002, *d* = 1.14) and FAST (see Figure 3c, HC$_{ep}$ vs. EP: *p* = .0002, *d* = 0.84 and HC$_{schz}$ vs. SCHZ: *p* < .0001, *d* = 1.30). The same differences appeared by using ATROPOS

Thalamic volume differences between groups

FIGURE 3 Global thalamic volume differences between patients with early psychosis and schizophrenia as compared with healthy controls. (a) Differences in the thalamic volume computed by FreeSurfer. (b–g) Differences in gray matter volume computed by NISEG, FAST, ATROPOS, ATROPOS-NOPV, SPM8 and SPM12, respectively. These volumes were computed by summing the *GMc* or *GMp* values of all the voxels contained in the refined thalamus masks and multiplying this sum by the voxel volume. Magenta and orange indicate PV-based and probability-based methods, respectively. Stars: in red, significance survived the FDR correction, and in black, significance that did not survive FDR correction

but did not survive the FDR correction (see Figure 3d). ATROPOS-NOPV revealed statistical differences only between SCHZ and their matched healthy subjects on the right thalamus (see Figure 3e, HC$_{schz}$ vs. SCHZ: p = .0003, d = 1.13). For both SPM8 and SPM12, a reduced GM volume in the right thalamus was observed in EP but not in SCHZ when compared with their respective control subjects. Only the differences obtained by SPM8 (p = .0017, 0.71) survived, however, the multiple comparisons correction. GM alterations were less prominent in the left thalamus. A decreased left thalamic GM volume was only identified in EP patients, and not in SCHZ, when using concentration based algorithms (NISEG: p < .001, d = 1.35), FAST: p = .0014, d = 0.72 and ATROPOS: p = .0024, d = 0.69).

4.2.2 | Relationship between total thalamus and GM volume and age

We then investigated how the total thalamic volume and the GM volume assessed by the six segmentation methods varied with age (Figure 4). Overall, the GM volume, but not the total thalamic volume,

changed significantly with age in both patients and controls. The nonlinear relationship between age and GM volume was best fitted with the quadratic model, particularly when the thalamic GM volume was assessed by NISEG.

4.3 | Thalamic subregions

Total volume—Nuclei volumes, based only on the binary masks derived from the thalamic parcellation, did not reveal any significant difference between groups (see Supplementary materials S2, Figure S1).

4.3.1 | Relationship between GM volume and age

As for the global thalamic GM volume (Figure 4), we found, overall, a decrease of GM volume with age for most of the thalamic subregions (Figure 5 for the pulvinar and Supplementary materials S3, Figures S2 to S7 for the rest of the thalamic nuclei). Interestingly, a separation

TABLE 2 Pair-wise differences in gray matter thalamic volume between early psychosis (n = 41) and schizophrenia patients (n = 23) compared with their respective matched healthy controls (n = 42 and n = 27, respectively)

	Healthy controls vs. early psychosis				Healthy controls vs. schizophrenia			
	Healthy controls Mean (SD)[a]	Early psychosis Mean (SD)[a]	t or U[b] (p value[c])	Cohen's d Mean (CI)[d]	Healthy controls Mean (SD)[a]	Schizophrenia Mean (SD)[a]	t or U[b] (p value[c])	Cohen's d Mean (CI)
Left hemisphere								
FreeSurfer	7.98(0.44)	7.81(0.56)	1.48(.1435)	0.323(0.320,0.326)	8.07(0.37)	8.19(0.83)	−0.67(.5035)	−0.190(−0.195,−0.186)
NISEG	4.02(0.33)	3.58(0.33)	6.13(**<.0001**)	1.347(1.345,1.350)	3.65(0.51)	3.47(0.44)	1.33(.1912)	0.383(0.379,0.388)
FAST	3.66(0.34)	3.38(0.42)	3.30(**.0014**)	0.728(0.725,0.731)	3.50(0.42)	3.31(0.35)	1.67(.1006)	0.482(0.478,0.486)
ATROPOS	4.13(0.36)	3.85(0.44)	3.14(**.0024**)	0.690(0.687,0.694)	3.73(0.51)	3.58(0.45)	1.12(.2666)	0.327(0.322,0.331)
ATROPOS-NOPV	3.88(0.44)	3.90(0.44)	−0.14(.8925)	−0.031(−0.034,−0.028)	3.27(0.60)	3.18(0.46)	0.52(.6032)	0.149(0.145,0.153)
SPM8	2.30(0.60)	2.02(0.54)	2.23(.0285)	0.497(0.494,0.500)	2.39(0.27)	2.32(0.31)	0.79(.4316)	0.230(0.226,0.234)
SPM12	4.36(0.40)	4.11(0.44)	2.70(.0084)	0.592(0.589,0.595)	4.24(0.37)	4.20(0.36)	0.41(.6801)	0.117(0.113,0.121)
Right hemisphere								
FreeSurfer	7.97(0.43)	7.74(0.66)	1.83(.0706)	0.403(0.400,0.406)	8.40(0.44)	7.91(0.64)	3.14(**.0029**)	0.908(0.903,0.912)
NISEG	3.63(0.32)	3.23(0.33)	5.64(**<.0001**)	1.240(1.237,1.243)	3.61(0.51)	3.12(0.33)	3.98(**.0002**)	1.142(1.138,1.146)
FAST	3.47(0.34)	3.19(0.32)	3.85(**.0002**)	0.844(0.841,0.847)	3.58(0.46)	3.05(0.35)	4.55(**<.0001**)	1.305(1.301,1.309)
ATROPOS	3.69(0.36)	3.47(0.44)	2.55(.0125)	0.560(0.557,0.563)	3.58(0.53)	3.24(0.38)	2.59(.0129)	1.167(1.163,1.171)
ATROPOS-NOPV	2.54(0.64)	2.78(0.55)	−1.83(.0716)	−0.398(−0.401,−0.395)	2.91(0.93)	2.08(0.46)	3.93(**.0003**)	1.125(1.121,1.129)
SPM8	2.51(0.46)	2.17(0.49)	3.24(**.0017**)	0.713(0.710,0.717)	2.38(0.29)	2.28(0.35)	1.10(.2769)	0.947(0.943,0.952)
SPM12	4.22(0.36)	4.03(0.36)	2.43(.0174)	0.534(0.531,0.537)	4.04(0.33)	3.84(0.42)	1.89(.0656)	1.077(1.073,1.082)

[a]Volume values are given in cm³. Mean (Standard Deviation).

[b]Comparisons between groups were conducted using the non-parametric Mann–Whitney U test or the parametric Student's t test. The applied test was based on the normality of data as evaluated by a Shapiro–Wilk test.

[c]p-values in bold remain significant after entering all uncorrected p-values (N = 12) into a False Discovery Rate (FDR) correction for multiple comparisons with q = 0.05.

[d]Confidence interval.

Relationship between the thalamic volume and age

FIGURE 4 Relationship between thalamic volume and age for healthy controls and patients with psychosis. (a) Left thalamic volume computed by the refined thalamus mask. (b–g) Left thalamic GM volume obtained by NISEG, FAST, ATROPOS, ATROPOS-NOPV, SPM8, and SPM12, respectively. (h) Right thalamic volume computed by the refined thalamus mask. (i–n) Right thalamic GM volume obtained by NISEG, FAST, ATROPOS, ATROPOS-NOPV, SPM8, and SPM12, respectively. Notes: Solid and dashed lines are the fitting curves for all control and all patients (EP and SCHZ jointly) respectively. Magenta and orange indicate the PV-based and the probability-based methods respectively

between the decay curves for both groups, particularly at early stages, is overall better depicted in the pulvinar and mediodorsal nuclei. Similarly than for the total thalamus GM volume (Figure 4), the best region-wise quadratic fit is overall obtained when using NISEG.

4.3.2 | Mean GM concentration and probability

We analyzed whether the mean GM within each of the thalamic subregions differed significantly between the patient groups and their respective control subjects. Significant correlations with age were found (Supplementary materials S1, Tables S1 and S2) when PV-based methods were used to compute the concentration values. Accordingly, the age was taken into account for the following group-wise study. On the contrary, we did not observe any significant correlation between mean GM (neither with GMc nor with GMp) and medication (Supplementary materials S1, Table S3). We did not observe any significant correlations with PANSS (positive, negative and general score). For this reason and to avoid the overadjustment effect, CPZ equivalents nor PANSS scores were not included as confounding variables in the model. GM differences between the pathological groups and their matched healthy controls emerged in some but not all thalamic subregions (Figures 6 and 7 illustrate the regions showing statistical differences). Detailed statistics are presented in Table 3 for NISEG and SPM12 and in the Supplementary material S4 (Tables S4 to S9) for the rest of the methods.

Overall, bilateral GM thalamic differences between groups are more pronounced when estimated by the tissue concentration as compared with the probability-based methods. Specifically, NISEG revealed the most extended GM differences between patient groups and their matched controls. After correcting for multiple comparisons, NISEG depicted statistically significant bilateral GM loss in the following thalamic regions of EP patients: pulvinar (left hemisphere: $p < .0001$, $d = 2.87$, right hemisphere: $p < .0001$, $d = 1.81$), medial pulvinar/centrolateral group (left hemisphere: $p < .0001$, $d = 1.03$, right hemisphere: $p < .0001$, $d = 1.55$), mediodorsal (left hemisphere: $p = .0002$, $d = 0.92$, right hemisphere: $p < .0001$, $d = 0.90$), and lateral posterior/ventral posterior group (left hemisphere: $p < .0001$, $d = 1.29$, right hemisphere: $p < .0001$, $d = 1.05$). In SCHZ patients however, only the right pulvinar ($p = .0075$, $d = 0.80$) and medial pulvinar/centrolateral group ($p = .0059$, $d = 0.82$) displayed a significant reduction of GM assessed with NISEG. ATROPOS and ATROPOS-NOPV also revealed a significant decrease of GM in the right thalamus of SCHZ patients (RH$_{ATROPOS}$: $p < .0031$, $d = 0.89$, RH$_{ATROPOS-NOPV}$: $p < .0026$, $d = 0.90$).
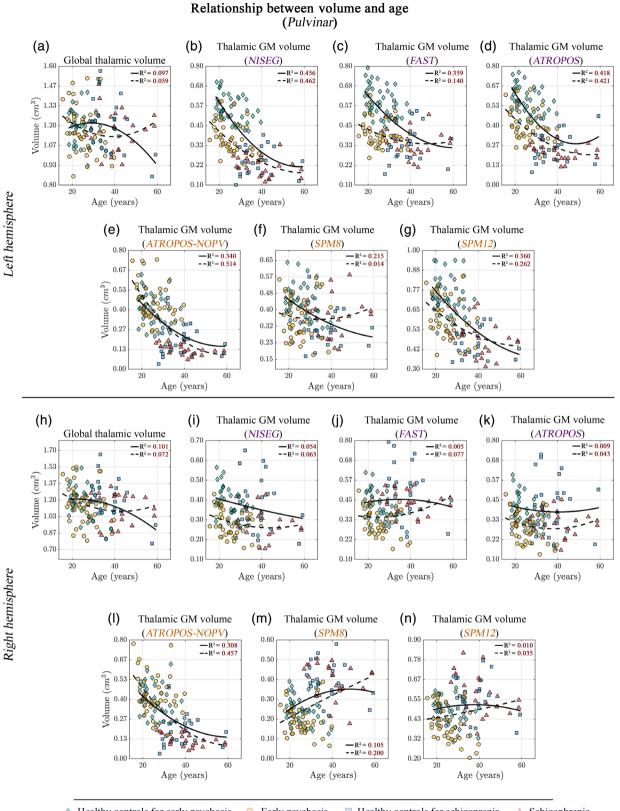
The other methods also indicated significant low GM in both right and left pulvinar of EP (LH$_{FAST}$: $p < .0001$, $d = 2.82$, RH$_{FAST}$: $p < .0001$, $d = 1.40$, LH$_{ATROPOS}$: $p < .0001$, $d = 2.31$, RH$_{ATROPOS}$: $p < .0001$, $d = 1.24$, LH$_{SPM8}$: $p < .0001$, $d = 1$, LH$_{SPM12}$: $p < .0001$, $d = 1.33$). We also found significant reduced GM for EP patients in the right lateral posterior/ventral posterior group using FAST and SPM8 ($p < .0001$, $d = 0.98$ and $p = .0016$, $d = 0.72$ respectively) and in

the right medial pulvinar/centrolateral group of patients using FAST ($p < .0001$, $d = 0.98$). However, these methods did not capture any significant GM alterations in the mediodorsal region of both patient groups.

4.4 | Voxel-wise analysis

VBM analyses revealed smaller GMc values within voxels from the posterior part of the thalamus in both EP and SCHZ as compared with their matched healthy subjects, even after correction for multiple comparisons (see Figure 8 for NISEG and Supplementary material S5, for FAST and ATROPOS). The affected voxels were mainly located in the right pulvinar cluster and the bilateral medial pulvinar/centrolateral group in SCHZ and EP, and also included the mediodorsal region in EP. No thalamic regions presented higher GMc values in patients compared with healthy controls. By contrast, after correction for multiple comparisons, no significant differences were found at voxel level when comparing the GMp maps of EP and SCHZ with their respective controls (see Figure 8 for SPM12 and Supplementary material S5, for ATROPOS-NOPV and SPM8). These results are in line with the findings obtained for the whole thalamus and the region-wise analyses, indicating that the GMc extracted from the NISEG method might represent a sensitive approach to detect subtle alterations in the thalamus of patients with psychosis.
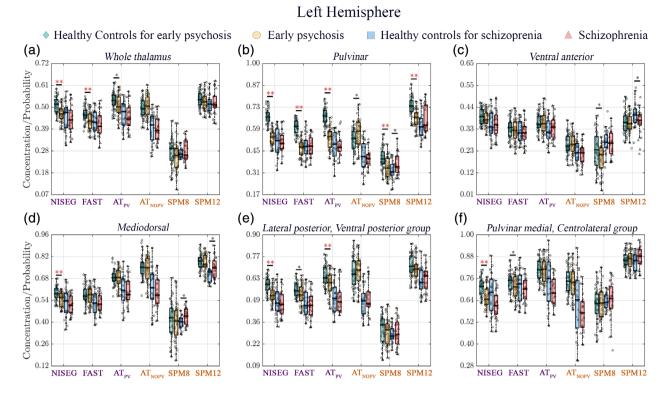
5 | DISCUSSION

To the best of our knowledge, this is the first study that explores partial volume effects in the GM analysis of the thalamus in early psychosis and schizophrenia patients. To do so, we employed six widely-used tissue segmentation approaches to assess GM alterations taking place during the course of schizophrenia, starting at early stages. We explored GM at three different anatomical scales: (a) whole thalamus, (b) thalamic subregions, and (c) thalamic voxels. The second original contribution of our work is the assessment in patients and controls of GM within seven thalamic nuclei or subregions derived from an atlas. Among the tissue segmentation techniques used, three of them (NISEG, FAST, ATROPOS) estimate the GM concentration by taking into account the partial volume effects while the others (ATROPOS-NOPV, SPM8, SPM12) are based on a posterior probability estimation to compute the GM probability. Notably, we found that these different approaches were not equivalent in detecting GM alterations in the thalamus of patients. Overall, the PV-based methodologies showed more sensitivity to capture differences between groups as compared with the probability-based approaches. Furthermore, in this work we promote the use of GM concentration weighted volumes as they revealed differences between the groups and significant changes with age while volume-based measures did not.
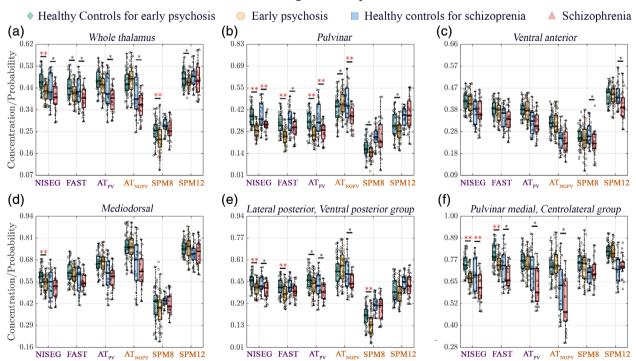
FIGURE 5 Relationship between the volume of the pulvinar and age for healthy controls and patients with psychosis. (a) Volume for the left pulvinar. (b–g) Left pulvinar GM volume obtained by NISEG, FAST, ATROPOS, ATROPOS-NOPV, SPM8 and SPM12, respectively. (h) Volume for the right pulvinar. (i–n) GM volume for the right pulvinar obtained by each of the segmentation methods. Notes: Solid and dashed lines are the fitting curves for all control and all patients (EP and SCHZ jointly) respectively. Magenta and orange indicate the PV-based and the probability-based methods, respectively
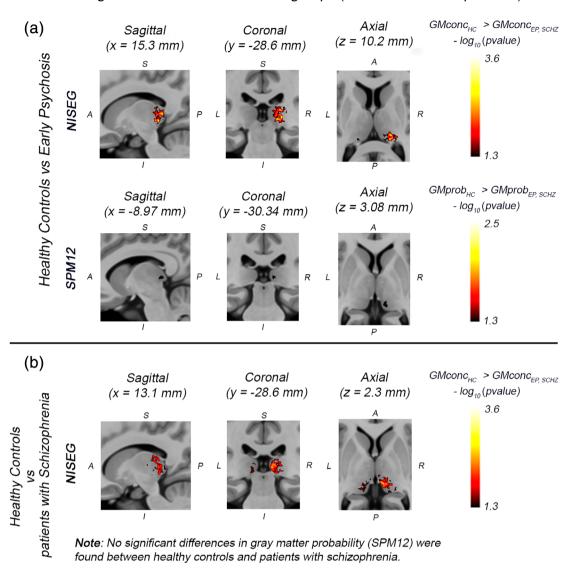
Left Hemisphere

FIGURE 6 Average GM estimated from either GM concentration (NISEG, FAST, ATROPOS) or GM posterior probability (ATROPOS-NOPV, SPM8, SPM12) within the left thalamus and its different thalamic nuclei in patients with psychosis (early psychosis and schizoprenia) and their respective matched control subjects. Note: Comparisons showing significant differences before and after correcting for multiple comparisons using FDR are highlighted with one black and two red asterisks, respectively. Magenta and orange indicate the PV-based and the probability-based methods respectively

Right Hemisphere

FIGURE 7 Average GM estimated from either GM concentration (NISEG, FAST, ATROPOS) or GM posterior probability (ATROPOS-NOPV, SPM8, SPM12) within the right thalamus and its different thalamic nuclei. Note: Comparisons showing significant differences before and after correcting for multiple comparisons using FDR are highlighted with one black and two red asterisks, respectively. Magenta and orange indicate the PV-based and the probability-based methods, respectively

TABLE 3 Pair-wise differences in gray matter concentration (NISEG) and probability (SPM12) within thalamic subregions between patients (early psychosis, EP, n = 41; schizophrenia, SCHZ, n = 23) and their respective control subjects (HC_EP, n = 42; HC_SCHZ, n = 27)

	Gray matter concentration (NISEG)				Gray matter probability (SPM12)			
	HC_EP vs. EP		HC_SCHZ vs. SCHZ		HC_EP vs. EP		HC_SCHZ vs. SCHZ	
	t or U[a] (p value)[b]	Cohen's d Mean(CI)[c]	t or U[a] (p value)[b]	Cohen's d Mean(CI)[c]	t or U[a] (p value)[b]	Cohen's d Mean(CI)[c]	t or U[a] (p value)[b]	Cohen's d Mean(CI)[c]
Left hemisphere								
Whole thalamus	5.39(**<.0001**)	1.187(1.184,1.190)	0.62(.5370)	0.181(0.176,0.185)	1.73(.0870)	0.382(0.379,0.386)	−0.22(.8255)	−0.063(−0.068,−0.059)
Pulvinar	13.09(**<.0001**)	2.876(2.873,2.880)	0.02(.9864)	0.007(0.003,0.011)	6.08(**<.0001**)	1.339(1.335,1.342)	−1.43(.1520)	−0.518(−0.522,−0.513)
Ventral anterior	1.04(.2970)	0.295(0.292,0.298)	−0.21(.8362)	−0.058(−0.062,−0.054)	0.25(.8043)	0.055(0.052,0.058)	2.03(.0478)	0.580(0.576,0.584)
Mediodorsal	3.78(**.0002**)	0.922(0.919,0.925)	0.41(.6815)	0.118(0.114,0.122)	1.21(.2284)	0.269(0.266,0.272)	−2.10(.0407)	−0.604(−0.608,−0.600)
Lateral posterior, ventral posterior	5.88(**<.0001**)	1.291(1.288,1.295)	0.62(.5376)	0.177(0.172,0.181)	1.51(.1357)	0.335(0.332,0.338)	−0.82(.4168)	−0.238(−0.242,−0.234)
Medial pulvinar, centrolateral	4.68(**<.0001**)	1.031(1.027,1.034)	1.97(.0543)	0.569(0.565,0.573)	−0.07(.9443)	−0.015(−0.018,−0.012)	−1.64(.1084)	−0.472(−0.477,−0.468)
Ventrolateral	1.89(.0627)	0.414(0.411,0.417)	−0.46(.6508)	−0.131(−0.136,−0.127)	0.06(.9554)	0.014(0.011,0.017)	−0.35(.7259)	0.062(0.058,0.066)
Ventral posterior, ventrolateral	3.81(**.0003**)	0.838(0.835,0.841)	0.29(.7715)	0.085(0.081,0.089)	−1.08(.2804)	−0.322(−0.325,−0.320)	−2.71(.0066)	−0.697(−0.702,−0.692)
Right hemisphere								
Whole thalamus	4.66(**<.0001**)	1.251(1.248,1.253)	2.15(.0313)	0.697(0.693,0.701)	2.10(.0392)	0.458(0.455,0.461)	0.92(.3637)	0.267(0.263,0.272)
Pulvinar	8.25(**<.0001**)	1.811(1.808,1.814)	2.79(**.0075**)	0.798(0.794,0.801)	2.83(.0059)	0.621(0.618,0.624)	−1.04(.3051)	−0.302(−0.307,−0.298)
Ventral anterior	0.50(.6190)	0.109(0.106,0.112)	0.39(.6960)	0.071(0.066,0.075)	0.33(.7401)	0.074(0.071,0.077)	2.50(.0161)	0.719(0.714,0.723)
Mediodorsal	4.11(**<.0001**)	0.902(0.899,0.906)	0.96(.3420)	0.275(0.271,0.279)	−0.21(.8321)	−0.049(−0.052,−0.045)	−0.40(.6894)	−0.117(−0.121,−0.113)
Lateral posterior, ventral posterior	4.77(**<.0001**)	1.047(1.044,1.050)	2.50(.0160)	0.717(0.712,0.721)	0.97(.3320)	0.272(0.269,0.275)	1.14(.2604)	0.326(0.321,0.330)
Medial pulvinar, centrolateral	7.07(**<.0001**)	1.552(1.549,1.556)	2.83(**.0059**)	0.824(0.820,0.828)	0.98(.3316)	0.212(0.209,0.215)	−1.20(.2376)	−0.343(−0.347,−0.339)
Ventrolateral	3.12(0.0025)	0.690(0.687,0.693)	0.82(.4168)	0.234(0.229,0.238)	2.72(.0079)	0.599(0.596,0.602)	1.04(.3049)	0.301(0.297,0.306)
Ventral posterior, ventrolateral	1.58(0.1179)	0.347(0.344,0.350)	1.53(.1332)	0.438(0.434,0.442)	−1.34(.1791)	−0.133(−0.136,−0.130)	−1.37(.1700)	−0.480(−0.484,−0.476)

[a]Comparisons between groups were conducted using the nonparametric Mann–Whitney U test or the parametric Student's t test. The applied test was based on the normality of data as evaluated by a Shapiro–Wilk test.

[b]p-values in bold remain significant after entering all uncorrected p-values (N = 16) into a False Discovery Rate (FDR) correction for multiple comparisons with q = 0.05.

[c]Confidence interval.

FIGURE 8 Local differences in GM concentration (NISEG) and probability (SPM12) between healthy controls and patients with psychosis revealed by the VBM analyses. (a) Significantly reduced gray matter concentration and probability in patients with early psychosis compared with healthy controls. (b) Significant decrease of gray matter concentration in patients with schizophrenia as compared with healthy controls. All the results were corrected for multiple comparisons using permutation tests and threshold free cluster enhancement

5.1 | Comparison between methods

There are important methodological differences in the way *GMc* and *GMp* maps are computed. The estimated tissue *concentration* and *probability* represent neither the same characteristic nor have the same underlying hypothesis about the observed intensity within a voxel. While *GMp* maps are weighted by prior probabilities from brain tissue atlases, no atlas prior drives the estimation of the PV concentration at each voxel. Such differences between *GMc* and *GMp* have been already reported by previous works assessing deep GM in multiple sclerosis (Bonnier et al., 2016). In our study, we can also observe that the actual histological GM pattern (see Figure 2a) resembles more the GM concentration than the GM probability. This suggests that PV

concentration performs better to capture subtle histological alterations, thus providing an improved method to detect focal GM atrophies within the thalamus of patients with early psychosis and chronic schizophrenia, even in small cohorts. From a theoretical point of view, it would be expected that a partial volume approach would be more precise than a probability-based strategy in brain regions with a mixture of GM and WM. For instance for the ventral posterior, ventrolateral group, which contains high density of crossing fibers, the GM probability is close to 0 (see Table 3 and Figure 2c). Despite the many methodological differences within the methods that estimate *GMc* (e.g., initialization or optimization strategy), these methods (particularly NISEG and FAST) show bigger effect sizes than the methods computing *GMp* (see Figures 6 and 7). We believe that the superior

sensitivity of NISEG and FAST is mainly driven by the fact they model the PV. The comparison between ATROPOS and ATROPOS-NOPV further corroborates the highest specificity when PV modeling is used, particularly when assessing the thalamic subregions.

Both SPM approaches (SPM8 and SPM12) are based on the same methodology but the GMp values and the subsequent volume estimation differ from each other. The values given by SPM12 tend to be higher than the values given by SPM8. We believe this effect might be caused by the use of different versions of the atlas priors (probabilistic spatial maps) for each SPM version. The GM probabilistic map employed in SPM12 spatially coincides more with the regions that are strongly penalized by the PV effect, causing an increase in the mean probability values in those regions. However, further studies with larger samples are needed to confirm these findings.

In regards to the whole thalamus, the GM volume is a more sensitive measure to capture differences between patients and controls, as compared with the volume of the refined FreeSurfer mask. The PV-based approach (in particular NISEG) was very efficient to depict GM loss in the thalamus of both EP and SCHZ. Likewise, we also found that the GM volume of the whole thalamus, but not the volume of the refined FreeSurfer mask, changes with age. Moreover, the quadratic relationship between GM volume and age was better (with both a good R^2 value and a well-differentiation between groups) when the GM volume was computed by using NISEG and ATROPOS as compared with the other methods evaluated. These analyses revealed a remarkable decline in GM volume with age in both patients and controls, with the GM loss being more pronounced between 20 and 30 years old than later in life.

When assessing the mean GM at subregion and voxel-wise levels, the concentration-based approaches (in particular NISEG and FAST) were also superior to the probability-based methods to detect GM alterations in patients. While all methods captured reduced GM in the pulvinar of EP patients, NISEG and FAST also revealed significant reduced GM in the mediodorsal, the medial pulvinar/centrolateral, and the lateral posterior/ventral posterior of EP and in the two sub-regions associated with the pulvinar in SCHZ. The hypothesis-based nature of the ROI-wise analyses makes it possible to search for differences in GMc or GMp in the subject anatomical space, without the need of interpolating the original gray-level intensity that would alter the PV at the voxel-level.

Differently, VBM analyses need to register the images to a reference space, which introduces an interpolation artifact in the intensity of those images. Despite this drawback, VBM can perform the statistical analysis without the requirement of a previously defined ROI. Interestingly and consistent with the region-wise analysis, VBM also revealed a significant GMc decrease mostly in the posterior part of the thalamus in EP and SCHZ patients compared with their matched controls.

Although the probability-based methods have been previously used to identify GM loss in patients with schizophrenia (Glahn et al., 2008; Pergola et al., 2015), these methods showed, in our study, only a few significant GM decrease at region-wise level (e.g., in pulvinar of EP) and did not captured focal loss in voxel-wise level,

neither in EP nor in SCHZ patients when compared with their matched controls.

5.2 | Regional GM alterations in the thalamus of early psychosis and chronic patients

The present study corroborates previous imaging data that the mediodorsal and posterior parts of the thalamus are particularly affected in schizophrenia (Janssen et al., 2012; Kemether et al., 2003). We provide however new insight about the nature and the dynamic of these alterations from the early phase of psychosis to the chronic stage.

In the following, we will primarily discuss the GM alterations found by NISEG and/or FAST as they appear to capture more finely and consistently thalamic differences between patients and controls. While we found only a significant decrease of GMc in the right pulvinar and medial pulvinar/centrolateral regions in SCHZ, lower GMc was observed in bilateral mediodorsal and pulvinar regions (pulvinar and medial pulvinar/centrolateral group), and lateral posterior/ventral posterior group of EP subjects. Based on the effect sizes (see Table 3 and Tables S4–S9), the significant GM alterations in bilateral mediodorsal and left pulvinar regions in EP, but not in SCHZ, cannot be explained by the larger EP cohort as compared with the SCHZ one. This strongly supports that the GMc in the mediodorsal and posterior parts of the thalamus in EP patients truly deviates from their age-matched healthy subjects and that GMc deficit is less pronounced in SCHZ patients. This latter was particularly evident in the left thalamus, both at the whole thalamus and at the region-wise levels.

A normalization effect by long-term medication as suggested for the thalamus size (Haijma et al., 2013) could be one explanatory factor. However in our study, the total volume of the thalamus was significantly smaller only in the right hemisphere of SCHZ, and not EP patients, when compared with their respective age-matched healthy subjects. Moreover, chlorpromazine equivalents did not correlate with GMc in any sub-regions.

The fact that GMc difference was more prominent in young EP than in older SCHZ patients may be linked to the age-dependent decrease of GMc which coincides with the developmental increase in WM volume (including tracts connected to the thalamus) until the age of 30 years (Lebel & Beaulieu, 2011). After this age, the GMc difference between SCHZ patients and control subjects tends to fade out most likely due to an accelerated alteration of WM integrity and volume following the first psychotic episode (Cetin-Karayumak et al., 2019; Peters & Karlsgodt, 2015). A significant finding of our study is therefore the presence of low GMc in the mediodorsal and posterior subregions of the thalamus early on along the course of the disorder. This early GM deficit is remarkably severe in the pulvinar, but less strong in the mediodorsal nucleus. This might explain why GMc remains significantly low in the pulvinar, but not mediodorsal region, of SCHZ patients as compared with their age-matched controls.

Noteworthy, our observation of reduced *GMc* localized in the right pulvinar, but not the mediodorsal region, of chronic patients corroborates postmortem data showing consistent decrease in volume/number of neurons in the right pulvinar but not so in the mediodorsal nucleus (Dorph-Petersen & Lewis, 2017). This further supports the idea that the estimated *GMc* based on PV modeling could represent a good imaging proxy for histological alterations.

Previous VBM analyses summarized by Pergola et al. (2015) indicate a focal loss of GM mostly centered around the mediodorsal nucleus in schizophrenia patients. Although our own VBM analyses identified focal decrease of *GMc* within the mediodorsal region, most of the voxels displaying significantly lower *GMc* were located in more posterior regions. This apparent discrepancy could arise from differences in terms of the clinical characteristics, age, and stage of the patients included in the cohorts, but also from the quality of age matching of the control subjects since we observed a strong nonlinear GM decline with age in both patients and healthy subjects.

5.3 | Limitations

As in any vivo imaging studies, the quality of the scans may have an influence on the results. However, an exhaustive quality control was performed to ensure that no artifacts could affect the segmentation results (for all tissue segmentation methods). Another important limitation of this study is the relatively small sizes of our cohorts. Therefore, such a study should be replicated in larger populations of patients. Despite this, some of the observed differences (e.g., in pulvinar of EP) are associated with remarkably large effect sizes.

6 | CONCLUSION

The strengths of our study include the investigation of two different cohorts (early and chronic stage of psychosis) with multiple tissue segmentation approaches and at different scales including at the thalamus nuclei level. Our study suggests that the PV model estimation of GM is very sensitive to detect focal GM atrophies within the thalamus of EP and SCHZ patients, even in relatively small cohorts. It reveals a remarkably robust GM deficit in the posterior part of the thalamus encompassing the pulvinar, particularly in EP. This study also provides a novel insight on the dynamic of GM alterations within the thalamus and its subregions. Thus, we observed a GM deficit in the mediodorsal nucleus of EP subjects (when compared with their matched controls), while the pulvinar displays reduced GM in both EP and SCHZ patients. Moreover, our exhaustive GM analyses point to alterations in a thalamic sub-region comprising the lateral posterior and ventral posterior nuclei. Applying the current approach in individuals At Risk Mental State (ARMS) will allow identifying whether these localized thalamic alterations, that are very pronounced during the early phase of psychosis, are already present during the prodromal stage. This information could therefore have a predictive value for the transition to psychosis.

Overall, our work promotes the use of PV-based methodologies for the study of local GM structural alterations within the thalamic nuclei in psychiatric disorders that is timely relevant and complementary to other existing studies based on structural or functional connectivity of the thalamus (Cho et al., 2018; Marenco et al., 2012; Woodward et al., 2012; Woodward & Heckers, 2016).

Finally, such assessment of GM integrity for the thalamus and its sub-divisions can also be relevant for other psychiatric disorders and beyond, as there is an increasing interest in the study of the thalamus in other neurological pathologies such as frontotemporal dementia, multiple sclerosis, and Parkinson's disease (Bisecco et al., 2019; Bocchetta et al., 2018; Tuleasca et al., 2018).

DATA AVAILABILITY STATEMENT

In order to ensure the reproducibility of our study, the individual gray matter concentration/probability images as well as the thalamic nuclei parcellations, in native and MNI spaces, are freely available in the following repository: 10.5281/zenodo.3760613. The demographic information table including age, gender and intracranial volume for each subject is also available.

ORCID

Yasser Alemán-Gómez https://orcid.org/0000-0001-6067-8639
Meritxell Bach Cuadra https://orcid.org/0000-0003-2730-4285

REFERENCES

Adriano, F., Spoletini, I., Caltagirone, C., & Spalletta, G. (2010). Updated meta-analyses reveal thalamus volume reduction in patients with first-episode and chronic schizophrenia. *Schizophrenia Research*, *123*(1), 1–14.

Andreasen, N. C., Pressler, M., Nopoulos, P., Miller, D., & Ho, B.-C. (2010). Antipsychotic dose equivalents and dose-years: A standardized method for comparing exposure to different drugs. *Biological Psychiatry*, *67*(3), 255–262.

Anticevic, A., Cole, M. W., Repovs, G., Murray, J. D., Brumbaugh, M. S., Winkler, A. M., ... Glahn, D. C. (2014). Characterizing thalamo-cortical disturbances in schizophrenia and bipolar illness. *Cerebral Cortex*, *24*(12), 3116–3130.

Ashburner, J., & Friston, K. J. (2005). Unified segmentation. *NeuroImage*, *26*(3), 839–851.

Association, A. P. (2000). *Diagnostic and statistical manual of mental disorders* (4th ed.) *Text Revision (DSM-IV-TR)*. Washington, DC: American Psychiatric Association.

Avants, B. B., Tustison, N. J., Wu, J., Cook, P. A., & Gee, J. C. (2011). An open source multivariate framework for n-tissue segmentation with evaluation on public data. *Neuroinformatics*, *9*(4), 381–400.

Avants, B. B., Yushkevich, P., Pluta, J., Minkoff, D., Korczykowski, M., Detre, J., & Gee, J. C. (2010). The optimal template effect in hippocampus studies of diseased populations. *NeuroImage*, *49*(3), 2457–2466.

Avram, M., Brandl, F., Bäuml, J., & Sorg, C. (2018). Cortico-thalamic hypo- and hyperconnectivity extend consistently to basal ganglia in schizophrenia. *Neuropsychopharmacology*, *43*(11), 2239–2248.

Battistella, G., Najdenovska, E., Maeder, P., Ghazaleh, N., Daducci, A., Thiran, J.-P., ... Fornari, E. (2017). Robust thalamic nuclei segmentation method based on local diffusion magnetic resonance properties. *Brain Structure & Function*, *222*(5), 2203–2216.

Baumann, P. S., Crespi, S., Marion-Veyron, R., Solida, A., Thonney, J., Favrod, J., ... Conus, P. (2013). Treatment and early intervention in psychosis program (TIPP-Lausanne): Implementation of an early intervention programme for psychosis in Switzerland. *Early Intervention in Psychiatry*, *7*(3), 322–328.

Benjamini, Y., & Hochberg, Y. (1995). Controlling the false discovery rate: A practical and powerful approach to multiple testing. *Journal of the Royal Statistical Society: Series B: Methodological*, *57*(1), 289–300.

Bisecco, A., Capuano, R., Caiazzo, G., d'Ambrosio, A., Docimo, R., Cirillo, M., ... Gallo, A. (2019). Regional changes in thalamic shape and volume are related to cognitive performance in multiple sclerosis. *Multiple Sclerosis Journal*, *3*, 135245851989255.

Bocchetta, M., Gordon, E., Cardoso, M. J., Modat, M., Ourselin, S., Warren, J. D., & Rohrer, J. D. (2018). Thalamic atrophy in frontotemporal dementia — Not just a C9orf72 problem. *NeuroImage: Clinical*, *18*, 675–681.

Bonnier, G., Kober, T., Schluep, M., Pasquier, R. D., Krueger, G., Meuli, R., ... Roche, A. (2016). A new approach for deep gray matter analysis using partial-volume estimation. *PLoS ONE*, *11*(2), e0148631.

Brugger, S. P., & Howes, O. D. (2017). Heterogeneity and homogeneity of regional brain structure in schizophrenia: A meta-analysis. *JAMA Psychiatry*, *74*(11), 1104–1111.

Buchmann, A., Dentico, D., Peterson, M. J., Riedner, B. A., Sarasso, S., Massimini, M., ... Ferrarelli, F. (2014). Reduced mediodorsal thalamic volume and prefrontal cortical spindle activity in schizophrenia. *NeuroImage*, *102*(Pt 2), 540–547.

Byne, W., Hazlett, E. A., Buchsbaum, M. S., & Kemether, E. (2009). The thalamus and schizophrenia: Current status of research. *Acta Neuropathologica*, *117*(4), 347–368.

Cetin-Karayumak, S., Biase, M. A. D., Chunga, N., Reid, B., Somes, N., Lyall, A. E., ... Kubicki, M. (2019). White matter abnormalities across the lifespan of schizophrenia: A harmonized multi-site diffusion MRI study. *Molecular Psychiatry*, 1–12.

Chan, R. C. K., Di, X., McAlonan, G. M., & Gong, Q.-y. (2011). Brain anatomical abnormalities in high-risk individuals, first-episode, and chronic schizophrenia: An activation likelihood estimation meta-analysis of illness progression. *Schizophrenia Bulletin*, *37*(1), 177–188.

Cho, K. I. K., Kwak, Y. B., Hwang, W. J., Lee, J., Kim, M., Lee, T. Y., & Kwon, J. S. (2019). Microstructural changes in higher-order nuclei of the thalamus in patients with first-episode psychosis. *Biological Psychiatry*, *85*(1), 70–78.

Choi, H. S., Haynor, D. R., & Kim, Y. (1991). Partial volume tissue classification of multichannel magnetic resonance images-a mixel model. *IEEE Transactions on Medical Imaging*, *10*(3), 395–407.

Cobia, D. J., Smith, M. J., Salinas, I., Ng, C., Gado, M., Csernansky, J. G., & Wang, L. (2017). Progressive deterioration of thalamic nuclei relates to cortical network decline in schizophrenia. *Schizophrenia Research*, *180*, 21–27.

Cropley, V. L., Klauser, P., Lenroot, R. K., Bruggemann, J., Sundram, S., Bousman, C., ... Zalesky, A. (2016). Accelerated gray and white matter deterioration with age in schizophrenia. *American Journal of Psychiatry*, *174*(3), 286–295.

Cuadra, M. B., Cammoun, L., Butz, T., Cuisenaire, O., & Thiran, J.-P. (2005). Comparison and validation of tissue modelization and statistical classification methods in T1-weighted MR brain images. *IEEE Transactions on Medical Imaging*, *24*(12), 1548–1565.

Danivas, V., Kalmady, S. V., Venkatasubramanian, G., & Gangadhar, B. N. (2013). Thalamic shape abnormalities in antipsychotic Naïve schizophrenia. *Indian Journal of Psychological Medicine*, *35*(1), 34–38.

de Boer, R., Vrooman, H. A., Ikram, M. A., Vernooij, M. W., Breteler, M. M., van der Lugt, A., & Niessen, W. J. (2010). Accuracy and reproducibility study of automatic MRI brain tissue segmentation methods. *NeuroImage*, *51*(3), 1047–1056.

Despotović, I., Goossens, B., & Philips, W. (2015). MRI segmentation of the human brain: Challenges, methods, and applications. *Computational and Mathematical Methods in Medicine*, *2015*, 1–23.

Dorph-Petersen, K.-A., & Lewis, D. A. (2017). Postmortem structural studies of the thalamus in schizophrenia. *Schizophrenia Research*, *180*, 28–35.

Evans, A. C., Janke, A. L., Collins, D. L., & Baillet, S. (2012). Brain templates and atlases. *NeuroImage*, *62*(2), 911–922.

Evans, A. C., Kamber, M., Collins, D. L., & MacDonald, D. (1994). An MRI-based probabilistic atlas of Neuroanatomy. In *Magnetic resonance scanning and epilepsy*, *NATO ASI series, pages* (pp. 263–274). Boston, MA: Springer.

Fischl, B., Salat, D. H., Busa, E., Albert, M., Dieterich, M., Haselgrove, C., ... Dale, A. M. (2002). Whole brain segmentation: Automated labeling of neuroanatomical structures in the human brain. *Neuron*, *33*(3), 341–355.

Fonov, V., Evans, A. C., Botteron, K., Almli, C. R., McKinstry, R. C., Collins, D. L., & Brain Development Cooperative Group. (2011). Unbiased average age-appropriate atlases for pediatric studies. *NeuroImage*, *54*(1), 313–327.

Glahn, D. C., Laird, A. R., Ellison-Wright, I., Thelen, S. M., Robinson, J. L., Lancaster, J. L., ... Fox, P. T. (2008). Meta-analysis of gray matter anomalies in schizophrenia: Application of anatomic likelihood estimation and network analysis. *Biological Psychiatry*, *64*(9), 774–781.

Glaister, J., Carass, A., NessAiver, T., Stough, J. V., Saidha, S., Calabresi, P. A., & Prince, J. L. (2017). Thalamus segmentation using multi-modal feature classification: Validation and pilot study of an age-matched cohort. *NeuroImage*, *158*, 430–440.

González Ballester, M. Á., Zisserman, A. P., & Brady, M. (2002). Estimation of the partial volume effect in MRI. *Medical Image Analysis*, *6*(4), 389–405.

Griffa, A., Baumann, P. S., Klauser, P., Mullier, E., Cleusix, M., Jenni, R., ... Hagmann, P. (2019). Brain connectivity alterations in early psychosis: From clinical to neuroimaging staging. *Translational Psychiatry*, *9*(1), 62.

Haijma, S. V., Van Haren, N., Cahn, W., Koolschijn, P. C. M. P., Hulshoff Pol, H. E., & Kahn, R. S. (2013). Brain volumes in schizophrenia: A meta-analysis in over 18 000 subjects. *Schizophrenia Bulletin*, *39*(5), 1129–1138.

Huang, P., Xi, Y., Lu, Z.-L., Chen, Y., Li, X., Li, W., ... Yin, H. (2015). Decreased bilateral thalamic gray matter volume in first-episode schizophrenia with prominent hallucinatory symptoms: A volumetric MRI study. *Scientific Reports*, *5*(1), 14505.

Iglesias, J. E., Insausti, R., Lerma-Usabiaga, G., Bocchetta, M., Van Leemput, K., Greve, D. N., ... Paz-Alonso, P. M. (2018). A probabilistic atlas of the human thalamic nuclei combining ex vivo MRI and histology. *NeuroImage*, *183*, 314–326.

Janssen, J., Alemán-Gómez, Y., Reig, S., Schnack, H. G., Parellada, M., Graell, M., ... Desco, M. (2012). Regional specificity of thalamic volume

deficits in male adolescents with early-onset psychosis. *The British Journal of Psychiatry*, 200(1), 30–36.

Jenkinson, M., Bannister, P., Brady, M., & Smith, S. (2002). Improved optimization for the robust and accurate linear registration and motion correction of brain images. *NeuroImage*, 17(2), 825–841.

Jenkinson, M., & Smith, S. (2001). A global optimisation method for robust affine registration of brain images. *Medical Image Analysis*, 5(2), 143–156.

Jones, E. G. (1985). *The thalamus*, New York, NY: Springer US.

Kay, S. R., Fiszbein, A., & Opler, L. A. (1987). The positive and negative syndrome scale (PANSS) for schizophrenia. *Schizophrenia Bulletin*, 13(2), 261–276.

Kemether, E. M., Buchsbaum, M. S., Byne, W., Hazlett, E. A., Haznedar, M., Brickman, A. M., ... Bloom, R. (2003). Magnetic resonance imaging of mediodorsal, pulvinar, and centromedian nuclei of the thalamus in patients with schizophrenia. *Archives of General Psychiatry*, 60(10), 983–991.

Klauser, P., Baker, S. T., Cropley, V. L., Bousman, C., Fornito, A., Cocchi, L., ... Zalesky, A. (2016). White matter disruptions in schizophrenia are spatially widespread and topologically converge on brain network hubs. *Schizophrenia Bulletin*, 43(2), 425–435.

Klein, A., Andersson, J., Ardekani, B. A., Ashburner, J., Avants, B., Chiang, M.-C., ... Parsey, R. V. (2009). Evaluation of 14 nonlinear deformation algorithms applied to human brain MRI registration. *NeuroImage*, 46(3), 786–802.

Koutsouleris, N., Gaser, C., Patschurek-Kliche, K., Scheuerecker, J., Bottlender, R., Decker, P., ... Meisenzahl, E. M. (2012). Multivariate patterns of brain-cognition associations relating to vulnerability and clinical outcome in the at-risk mental states for psychosis. *Human Brain Mapping*, 33(9), 2104–2124.

Lebel, C., & Beaulieu, C. (2011). Longitudinal development of human brain wiring continues from childhood into adulthood. *The Journal of Neuroscience*, 31(30), 10937–10947.

Maggioni, E., Crespo-Facorro, B., Nenadic, I., Benedetti, F., Gaser, C., Sauer, H., ... ENPACT group. (2017). Common and distinct structural features of schizophrenia and bipolar disorder: The European network on psychosis, affective disorders and cognitive trajectory (ENPACT) study. *PLoS ONE*, 12(11), e0188000.

Manjón, J. V., Tohka, J., & Robles, M. (2010). Improved estimates of partial volume coefficients from noisy brain MRI using spatial context. *NeuroImage*, 53(2), 480–490.

Marenco, S., Stein, J. L., Savostyanova, A. A., Sambataro, F., Tan, H.-Y., Goldman, A. L., ... Weinberger, D. R. (2012). Investigation of anatomical Thalamo-cortical connectivity and fMRI activation in schizophrenia. *Neuropsychopharmacology*, 37(2), 499–507.

Morel, A., Magnin, M., & Jeanmonod, D. (1997). Multiarchitectonic and stereotactic atlas of the human thalamus. *Journal of Comparative Neurology*, 387(4), 588–630.

Najdenovska, E., Alemán-Gómez, Y., Battistella, G., Descoteaux, M., Hagmann, P., Jacquemont, S., ... Bach Cuadra, M. (2018). In-vivo probabilistic atlas of human thalamic nuclei based on diffusion- weighted magnetic resonance imaging. *Scientific Data*, 5, 180270.

Noe, A., & Gee, J. C. (2001). Partial volume segmentation of cerebral MRI scans with mixture model clustering. In M. F. Insana & R. M. Leahy (Eds.), *Information Processing in Medical Imaging, lecture notes in computer science* (pp. 423–430). Berlin Heidelberg: Springer.

Okada, N., Fukunaga, M., Yamashita, F., Koshiyama, D., Yamamori, H., Ohi, K., ... Hashimoto, R. (2016). Abnormal asymmetries in subcortical brain volume in schizophrenia. *Molecular Psychiatry*, 21(10), 1460–1466.

Otsu, N. (1979). A threshold selection method from gray-level histograms. *IEEE Transactions on Systems, Man, and Cybernetics*, 9(1), 62–66.

Pergola, G., Selvaggi, P., Trizio, S., Bertolino, A., & Blasi, G. (2015). The role of the thalamus in schizophrenia from a neuroimaging perspective. *Neuroscience and Biobehavioral Reviews*, 54, 57–75.

Pergola, G., Trizio, S., Di Carlo, P., Taurisano, P., Mancini, M., Amoroso, N., ... Blasi, G. (2017). Grey matter volume patterns in thalamic nuclei are

associated with familial risk for schizophrenia. *Schizophrenia Research*, 180, 13–20.

Peters, B. D., & Karlsgodt, K. H. (2015). White matter development in the early stages of psychosis. *Schizophrenia Research*, 161(1), 61–69.

Puonti, O., Iglesias, J. E., & Van Leemput, K. (2016). Fast and sequence-adaptive whole-brain segmentation using parametric Bayesian modeling. *NeuroImage*, 143, 235–249.

Qiu, A., Zhong, J., Graham, S., Chia, M. Y., & Sim, K. (2009). Combined analyses of thalamic volume, shape and white matter integrity in first-episode schizophrenia. *NeuroImage*, 47(4), 1163–1171.

Roche, A. (2016). Niseg: Standalone image segmentation package - will supersede nipy.algorithms.segmentation. https://github.com/alexis-roche/niseg.

Roche, A., & Forbes, F. (2014). Partial volume estimation in brain MRI revisited. In *Medical Image Computing and Computer-Assisted Intervention – MICCAI 2014, lecture notes in computer science* (pp. 771–778). Cham: Springer.

Rohde, G. K., Barnett, A. S., Basser, P. J., Marenco, S., & Pierpaoli, C. (2004). Comprehensive approach for correction of motion and distortion in diffusion-weighted MRI. *Magnetic Resonance in Medicine*, 51(1), 103–114.

Rosen, B., Toga, A., and Weeden, V. J. (2012). Human Connectome Project | Data.

Schaltenbrand, G., Hassler, R. G., & Wahren, W. (1977). *Atlas for Stereotaxy of the human brain* (5002156). Stuttgart, Germany: Thieme.

Shattuck, D. W., Sandor-Leahy, S. R., Schaper, K. A., Rottenberg, D. A., & Leahy, R. M. (2001). Magnetic resonance image tissue classification using a partial volume model. *NeuroImage*, 13(5), 856–876.

Sherman, S. M., & Guillery, R. W. (2006). *Exploring the thalamus and its role in cortical function* (956663203). Cambridge, MA. OCLC: MIT Press.

Smith, M. J., Wang, L., Cronenwett, W., Mamah, D., Barch, D. M., & Csernansky, J. G. (2011). Thalamic morphology in schizophrenia and schizoaffective disorder. *Journal of Psychiatric Research*, 45(3), 378–385.

Steullet, P. (in press). Thalamus-related anomalies as candidate mechanism-based biomarkers for psychosis. *Schizophrenia Research*, S0920-9964(19), 30203–30208.

Su, J. H., Thomas, F. T., Kasoff, W. S., Tourdias, T., Choi, E. Y., Rutt, B. K., & Saranathan, M. (2019). Thalamus optimized multi atlas segmentation (THOMAS): Fast, fully automated segmentation of thalamic nuclei from structural MRI. *NeuroImage*, 194, 272–282.

Sullivan, E. V., Rosenbloom, M., Serventi, K. L., & Pfefferbaum, A. (2004). Effects of age and sex on volumes of the thalamus, pons, and cortex. *Neurobiology of Aging*, 25(2), 185–192.

Tohka, J. (2014). Partial volume effect modeling for segmentation and tissue classification of brain magnetic resonance images: A review. *World Journal of Radiology*, 6(11), 855–864.

Tohka, J., Dinov, I. D., Shattuck, D. W., & Toga, A. W. (2010). Brain MRI tissue classification based on local Markov random fields. *Magnetic Resonance Imaging*, 28(4), 557–573.

Tohka, J., Zijdenbos, A., & Evans, A. (2004). Fast and robust parameter estimation for statistical partial volume models in brain MRI. *NeuroImage*, 23(1), 84–97.

Tournier, J.-D., Calamante, F., & Connelly, A. (2012). MRtrix: Diffusion tractography in crossing fiber regions. *International Journal of Imaging Systems and Technology*, 22(1), 53–66.

Tuleasca, C., Régis, J., Najdenovska, E., Witjas, T., Girard, N., Bolton, T., ... Van de Ville, D. (2018). Pretherapeutic resting-state fMRI profiles are associated with MR signature volumes after stereotactic radiosurgical thalamotomy for essential tremor. *Journal of Neurosurgery*, 129(Suppl1), 63–71.

Tustison, N. J., Avants, B. B., Cook, P. A., Zheng, Y., Egan, A., Yushkevich, P. A., & Gee, J. C. (2010). N4ITK: Improved N3 bias correction. *IEEE Transactions on Medical Imaging*, 29(6), 1310–1320.

van den Heuvel, M. P., Sporns, O., Collin, G., Scheewe, T., Mandl, R. C. W., Cahn, W., … Kahn, R. S. (2013). Abnormal Rich Club organization and functional brain dynamics in schizophrenia. *JAMA Psychiatry*, *70*(8), 783–792.

van Erp, T. G. M., Hibar, D. P., Rasmussen, J. M., Glahn, D. C., Pearlson, G. D., Andreassen, O. A., … Turner, J. A. (2016). Subcortical brain volume abnormalities in 2028 individuals with schizophrenia and 2540 healthy controls via the ENIGMA consortium. *Molecular Psychiatry*, *21*(4), 547–553.

Van Leemput, K., Maes, F., Vandermeulen, D., & Suetens, P. (1999). Automated model-based tissue classification of MR images of the brain. *IEEE Transactions on Medical Imaging*, *18*(10), 897–908.

Woodward, N. D., & Heckers, S. (2016). Mapping Thalamocortical functional connectivity in chronic and early stages of psychotic disorders. *Biological Psychiatry*, *79*(12), 1016–1025.

Woodward, N. D., Karbasforoushan, H., & Heckers, S. (2012). Thalamocortical Dysconnectivity in schizophrenia. *American Journal of Psychiatry*, *169*(10), 1092–1099.

Yung, A. R., Yuen, H. P., McGorry, P. D., Phillips, L. J., Kelly, D., Dell'Olio, M., … Buckby, J. (2005). Mapping the onset of psychosis: The comprehensive assessment of at-risk mental states. *The Australian and New Zealand Journal of Psychiatry*, *39*(11–12), 964–971.

Zhang, J. (1993). The mean field theory in EM procedures for blind Markov random field image restoration. *IEEE Transactions on Image Processing*, *2*(1), 27–40.

Zhang, Y., Brady, M., & Smith, S. (2001). Segmentation of brain MR images through a hidden Markov random field model and the expectation-maximization algorithm. *IEEE Transactions on Medical Imaging*, *20*(1), 45–57.

SUPPORTING INFORMATION

Additional supporting information may be found online in the Supporting Information section at the end of this article.